Influence of Halide Substitution and External Stimuli on Ion Transport in Inverted $MAPb(I_{1-x}Br_x)_3$ Perovskite Solar Cells

Hamza Javaid,[†] Christie L.C. Ellis,[†] Emily C. Smith,[†] Yao Liu,[⊥,§] Monojit Bag,[‡] and D. Venkataraman*[,†]

[†] Department of Chemistry, University of Massachusetts Amherst, Amherst, Massachusetts 01003-9303, United States

[⊥] Department of Polymer Science and Engineering, University of Massachusetts Amherst, Amherst, Massachusetts 01003-9303, United States

[‡] Department of Physics, Indian Institute of Technology Roorkee, Roorkee, Uttarakhand 247667, India

ABSTRACT

The coupled electronic-ionic response in various $MAPb(I_{1-x}Br_x)_3$-based inverted perovskite solar cells (PSCs) is studied *in-operando* by impedance spectroscopy (IS) under varied AM1.5G light intensities and electrical biases. We show that the concentration of Br^- in the composition significantly alters the capacitance and resistive response of the PSC under external stimuli. For example, we observed that the low frequency capacitance does not increase proportionally with light intensity, instead it is highly dependent on the amount of Br^- in the composition. We found

that the recombination resistance (R_{rec}) has a linear inverse relationship with light intensity in $MAPbI_3$ and $MAPbBr_3$ whereas, the mixed compositions show deviation. Interestingly, the deviation of R_{rec} from linearity also scales with the increase in Br^- concentration. Upon applying an electrical bias, a large deviation of R_{rec} from linearity was observed all mixed halide compositions exhibited a non-linear inverse trend. We further report the diffusion coefficient (*D*) for each $MAPb(I_{1-x}Br_x)_3$ composition under different light intensity. Notably, the *D* values decreased on changing the composition from $MAPbI_3$ (10^{-7} cm^2 s^{-1}) to $MAPb(I_{0.8}Br_{0.2})_3$ and $MAPbBr_3$ (10^{-8} cm^2 s^{-1}). On the other hand, mixed compositions containing more than 20% Br^- concentration show faster diffusion kinetics. Overall, our results emphasize on the complex and intertwined nature of electronic and ionic response in PSC that is tunable by changing the halide composition.

INTRODUCTION

Light-induced ion migration has been widely observed in hybrid organic-inorganic perovskites (HOIPs).[1–4] However, the implications of light-induced ion transport on device performance remain unclear.[5] For example, the instability of HOIPs under prolonged exposure to light has been attributed to ion migration,[6] and yet, self-healing induced by ion migration under cycled illumination may increase the short-term stability.[7] Although the mobility of A- and B-site ions is still an ongoing debate, there has been agreement on the transport of halide ions under illumination.[8] Various experimental and theoretical studies suggest that halide migration is dependent on the HOIP composition, but a systematic study to quantify this effect is still lacking.[9]

Mixed halide HOIPs employing I^- and Br^- have been extensively employed in perovskite solar cells (PSCs). The halide ratio in $MAPb(I_{1-x}Br_x)_3$ is often modified to achieve a required band-gap

or to improve a structural stability which is vital for improving the device performance.[10] However, changing the composition influences the halide migration hence, their distribution in the perovskite film. For example, in mixed I^- and Br^- compositions, the Br^- ions have lower activation energy (E_A) barrier for migration compared to I^-,[11] therefore, they typically located near the interfaces and grain boundaries.[12,13] Although, ion migration has become a popular feature of PSCs, further experimental studies are required to understand the fundamental nature and implications of this phenomenon. Previous studies have linked ion migration with illumination and electrical bias,[10,14,15] but the influence of halide composition on ion migration has been widely overlooked. Similarly, the interplay between the halide composition, ion migration, illumination and electrical bias needs to be studied to hone our understanding about these peculiar yet remarkable photovoltaic materials.

Herein, we report a detailed impedance spectroscopy (IS) analysis of different p-i-n $MAPb(I_{1-x}Br_x)_3$-based devices *in-operando* under variable AM1.5G illumination intensities and electrical bias. We found that the concentration of Br^- in the composition significantly alter the capacitance and resistive response under varying light intensity and electrical bias. We observed that the high frequency electronic response is coupled with the low frequency ionic responses, hence, they cannot be analyzed independently. However, the low frequency capacitance, unlike previous reports, did not increase proportionally with light intensity.[16,17] Instead, the increase in capacitance with light intensity was accompanied by the shift of capacitance curve towards higher frequencies. Notably, this effect is more significant in Br^- containing compositions. Furthermore, we show that the recombination resistance (R_{rec}) has a linear inverse relationship with light intensity in $MAPbI_3$ and $MAPbBr_3$ whereas, the mixed compositions deviate from the linearity. This deviation becomes more pronounced with the increase in Br^- concentration. Similar to the effect of light intensity, the slope of R_{rec} vs electrical bias plot increases for low Br^- compositions *i.e.* $MAPb(I_{0.8}Br_{0.2})_3$ and

$MAPb(I_{0.6}Br_{0.4})_3$. Thus, we surmise that a large Br^- concentration is favorable for charge screening. Furthermore, we calculated the ionic diffusion coefficient (*D*) for each $MAPb(I_{1-x}Br_x)_3$ composition under different light intensity and found that the *D* values decreased on changing the composition from $MAPbI_3$ (10^{-7} cm^2 s^{-1}) to $MAPbBr_3$ (10^{-8} cm^2 s^{-1}). We present a detailed analysis and complete picture of how the ion transport properties evolve with I/Br ratio in $MAPb(I_{1-x}Br_x)_3$ devices under different illumination intensities and electrical biases.

EXPERIMENTAL SECTION

Device fabrication. ITO-coated glass substrates (20 ± 5 ohms sq^{-1}) were obtained from Thin Film Devices Inc. and were cleaned by ultrasonication in detergent, water, acetone and isopropyl alcohol for 10 min each. Poly(benzothiadiazole vinylene-alt-2,5-bis(4-sodium sulfonate)butoxy)-1,4-phenylenevinylene) (PVBT-SO_3) (see structure, Figure S8a) was dissolved in water and then spin coated atop of ITO coated glass substrate at 3500 rpm. No thermal annealing was performed post-spin coating. For $MAPbI_3$ and $MAPbBr_3$ devices, a 1.4 M precursor solution of MAI/MABr (Dyesol) and PbI_2/$PbBr_2$ (Sigma Aldrich) (1:1) in gamma-butyrolactone (GBL)/dimethyl sulfoxide (DMSO) (v/v 7:3) was prepared and stirred overnight. For mixed halide perovskites, the concentration of Br^- was increased by adjusting the relative mole rations of MAI, MABr, $PbBr_2$, and PbI_2 accordingly. The precursor solutions were then spin coated on the HTM by a two-step spin-coating procedure: 1500 rpm for 20 s and 2000 rpm for 60 s. During the second step, chlorobenzene (antisolvent) was dripped onto the substrate after 20 s. As-cast films were left at room temperature for 1 min followed by thermal annealing at 100 °C for 5 min inside the N_2-filled glovebox (<1 ppm of O_2, <1 ppm of H_2O). A solution of Phenyl-C_{61}-butyric acid methyl ester ($PC_{61}BM$) (20 mg ml^{-1}) in chlorobenzene was spin coated atop the perovskite layer at 1000 rpm

for 60 s. Then, C_{60}-N (3 mg mL^{-1}) (see structure, Figure S8b) in 2,2,2-Trifluoroethanol (TFE) was spin coated at 4000 rpm to give a 15 nm film. Finally, 100 nm Ag metal (6 mm^2) was thermally deposited onto the active layer under high vacuum (2 x 10^{-6} mbar).

Characterization. The *J-V* studies were conducted inside the N_2-filled glovebox under AM1.5G (100 mW cm^{-2}) irradiation using Newport 91160 300-W solar simulator. All *J-V* scans were obtained from –0.5 to 1.5 V at a scan rate of ~0.26 V s^{-1}. The light intensity was adjusted using NREL-calibrated Si solar cell with a KG-5 filter. For intensity-dependent measurements, power was varied, and the resulting intensity was calibrated. Before each measurement, the device was left in the dark for 5 min to avoid degradation from extended light exposure.

Electrochemical impedance measurements were conducted using Agilent 4294A Precision Impedance Analyzer under varying light intensities of AM1.5G at short-circuit condition under constant 50 mV AC amplitude. The frequency was swept from 1 MHz to 40 Hz, and the resulting response was fit from 0.2 MHz to 100 Hz. Before every IS measurement under different light intensity, the device was left in the dark for ~2 min to minimize the effect of previous scan.

Powder X-ray diffraction (PXRD) measurements were carried out on perovskite samples coated on clean glass substrates with a PANalytical X'Pert3 X-ray diffractometer having a Ni filter, 1/2 in. diverging slit, vertical goniometer, and X'Celerator detector. Measurements were taken from $2\theta = 10°$ to 50° under Cu Kα (1.542 Å).

RESULTS AND DISCUSSION

We fabricated $MAPb(I_{1-x}Br_x)_3$-based p-i-n devices where x= 0, 0.2, 0.4, 0.6, 0.8 and 1.0. Powder x-ray diffraction pattern confirmed the formation of the three-dimensional perovskite in each of these compositions. We observed a shift from a tetragonal (*I*4/*mcm*) to a cubic ($Pm\bar{3}m$)

structure when we changed the composition from $MAPbI_3$ to $MAPbBr_3$, consistent with the reported structure for each compound (SI Figure S1).[18,19]

We employed the IS to study the electronic and ionic capacitive responses in different $MAPb(I_{1-x}Br_x)_3$ compositions *in-operando*. In IS measurements, the impedance was measured by applying a 20 mV AC voltage whose frequency was swept from 300 kHz to 40 Hz. The scan time was limited to 30 sec, minimizing the effects of non-steady-state conditions. Each composition was exposed to different light intensities in order to study the composition dependent capacitive response. The capacitive response of PSC can be divided into three distinct frequency regimes namely, low ($f < 100$ Hz), intermediate (100 Hz $< f < 0.1$ MHz), and high ($f > 0.1$ MHz).[20] The high and intermediate frequency is often related to the chemical capacitance and dipole contributions,[21] respectively, whereas the low frequency response represents the electrode polarization due to the accumulation of charges[22] and ion migration.[23] As shown in **Figure 1**, the high frequency capacitance does not change with light intensity hence, it can be treated as a geometric capacitance. Such independent response of high frequency capacitance on light intensity was also observed by Pockett and co-workers.[21] Conversely, the intermediate and low frequency capacitance increased significantly with increasing light intensity. Upon plotting the low frequency capacitance per unit length against light intensity for $MAPbI_3$, $MAPb(I_{0.8}Br_{0.2})_3$ and $MAPbBr_3$ resulted in a slope of 0.5, 0.48, and 0.87, respectively (**Figure 2**). This data shows that the low frequency capacitance does not increase proportionally with the light intensity, hence, this observation is inconsistent with the origin of the measured capacitance arising from photogenerated charges in the HOIP layer. This subjugates some previous studies that have reported a proportional increase in low frequency capacitance with increasing light intensity.[16,17] We surmise that the difference in the observation could be due to the different perovskite

composition, device architecture, morphology and fabrication method. Our results support the complex nature of the capacitance in perovskite solar cells which was suggested by Pockett and co-workers.[24] Rather than treating the capacitance as purely electronic, we believe that it originates due to coupled electronic-ionic relaxations where the distribution of ionic vacancies can modify the electronic impedance. A similar observation was reported by Moia and co-workers.[25] Here, it is important to mention that the ionic environment is entirely dependent on the composition of perovskite. Since we are changing the ratio of halide ions in $MAPb(I_{1-x}Br_x)_3$, both the nature and number of ionic vacancies would vary.

In our previous work, we showed that the low frequency capacitance was modulated under an electrical bias.[26] Here, we extended our analysis to study the nature of the low frequency capacitance upon changing the halide composition in $MAPb(I_{1-x}Br_x)_3$ under applied bias. The low frequency capacitance showed an increase with the applied bias in each composition **(Figure 3)**. This increase in capacitance under electrical bias was larger in magnitude compared to the enhancement observed upon increasing light intensity. We hypothesize that the photogenerated charges and mobile ionic defects scale with the applied bias. This is different from the effect of light intensity where only the density of free carriers is altered.[2] We also monitored the capacitance per unit length at 100 Hz under different applied bias in different halide compositions **(Figure 4)**. In general, the capacitance does not change at lower applied biases but increases drastically at biases above 500 mV. To understand this we employed the model that was proposed by our group previously.[26] The capacitance increases when the sum of applied bias (V_{App}) and photovoltage (V_{Ph}) exceeds the built-in voltage (V_{bi}) of a device. In this situation, the ionic defects also screen the charges and prevent recombination.

The fact that both light intensity and bias have similar effect on the low frequency capacitance indicate that the electronic and ionic processes are coupled. To test our hypothesis, we changed the bias and light intensity simultaneously for $MAPb(I_{0.8}Br_{0.2})_3$ composition. We found under low light intensity, there was a significant increase in the capacitance at biases >500 mV. When the light intensity was increased, a lower magnitude of bias was required to induce this same capacitance increase (Figure S2). Doubling the light intensity shifts the knee to a lower bias by ~46 mV. This shift correlates with the increase in V_{Ph} with light intensity that can overcome the V_{bi} at a lower V_{App}.

To investigate the interdependence of ionic distribution and charge recombination, we plotted the electronic recombination resistance (R_{rec}), extrapolated from the high-frequency regime of IS data, against light intensity for each $MAPb(I_{1-x}Br_x)_3$ composition. For $MAPbI_3$ and $MAPbBr_3$, the R_{rec} had a linear inverse relationship with light intensity with a slight deviation from linearity (**Figure 5**). This linear inverse relationship could be expected from a PSC, provided that the dark and light responses of a cell are additive.[21] Notably, for mixed halide compositions, there is more deviation from the linearity of these plots, the slope of which scales with the increase in the Br^- concentration. The slope changes from -0.65 in $MAPb(I_{0.8}Br_{0.2})_3$ to -0.17 in $MAPb(I_{0.2}Br_{0.8})_3$. A possible explanation for this observation is the favorable screening of charges by the Br^- defects. As the concentration of Br^- defects increase, the probability of charge recombination decreases even upon increasing light intensity. Therefore, the decrease in R_{rec} is not very significant in $MAPb(I_{0.2}Br_{0.8})_3$ and $MAPb(I_{0.4}Br_{0.6})_3$ (Figure 5). Due to the well documented phase segregation effect in mixed halide HOIPs, it is safe to assume that halide defects are dominant in mixed compositions compared to the pristine ones hence, the latter follow linearity with light intensity. This is intuitive because the phase segregation in mixed halide compositions could cause an

inhomogeneous distribution of ions in the film thus, increasing the possibility of point defects due to the lack of stoichiometry.

We also plotted the R_{rec} as a function of applied bias. Unlike R_{rec} vs intensity plot, the curves exhibited a non-linear decrease upon increasing electrical bias (Figure S3). This is due to the increased contribution of ionic defects under bias compared to light intensity. Similar to the effect of light intensity on R_{rec}, the rate of decrease in R_{rec} is higher in low Br^- compositions *i.e.* $MAPb(I_{0.8}Br_{0.2})_3$ and $MAPb(I_{0.6}Br_{0.4})_3$. The compositions containing larger Br^- concentration (x> 0.4) show less decrease in R_{rec}.

The IS data for $MAPb(I_{1-x}Br_x)_3$ compositions under different light intensities (Figure S4) was fitted with an equivalent circuit model that we have already developed.[23,27] The linear response in the low-frequency part of the Nyquist plot followed by a curvature back towards the real axis (Figure S6a) was modeled with a Warburg element, which is characteristic of mass diffusion to either a reactive or adsorbing boundary.[28] The fitted data for $MAPbI_3$ and $MAPbBr_3$ is shown in Figure S5a and 5c, and the corresponding values for each element are tabulated in Tables S1 and S3. In previous reports, we associated the Warburg response with the diffusion of methylammonium (MA^+) in $MAPbI_3$ because the impedance response changed as a function of organic cation substitution.[29] This observation was also corroborated by Maier and co-workers.[2] The MA^+ migration has also been reported by other groups.[30] Additionally, computational studies indicate that iodide migration occurs on timescales <μs, much lower than the ms timescale in which we observe the Warburg response.[29] Conversely, numerous groups interpret it as a halide diffusion.[8,31,32] Analysis of the Warburg component provides us information about ion diffusion both to the interfaces as well as through the bulk because, in case of thin films, length of the depletion zone approaches the active layer thickness. $MAPbI_3$ devices show mass diffusion to an

adsorbing boundary, while $MAPbBr_3$ devices exhibit semi-infinite diffusion in the frequency range analyzed (Figure 5c). The ionic diffusion coefficients (D) can be calculated using the Warburg time constant (T_w) values from the Warburg impedance equation and the relationship:[23]

$$D = \frac{{L_D}^2}{T_w}$$

where L_D ~300 nm, the film thickness as measured by profilometry. The T_w values for $MAPbI_3$ and $MAPbBr_3$ are ~0.0047 s and ~0.018 s, respectively, under 1 Sun illumination intensity. To validate our data, we also calculated the Warburg time constant for $MAPbI_3$ from the characteristic ankle frequency between the capacitive and Warburg domains in the low frequency IS response as reported by Bisquert and co-workers.[33] The time constants calculated from our model match well with the ones calculated using their method (Table S5). This comparison further validates our model.

The D values scale with light intensity in $MAPbI_3$ due to an increase in the photogenerated field that favors the migration of positive/negative charged defects towards the contact layers where they get stabilized by charge carrier accumulation (**Figure 6**). Such stabilization of defects provides the driving force for migration towards the electrodes. As shown in Figure 6, D values in $MAPbBr_3$ do not show a significant change with increasing light intensity. This trend could be understood using the defect migration model proposed by DeAngelis and co-workers.[29] Under illumination, the photogenerated field causes vacancies to move towards interfaces which in turn creates an electrostatic potential gradient across the perovskite that opposes the field. In case of $MAPbBr_3$, the Br^- related defects can reach selective contacts on very short timescales and generate a strong internal field to compensate the photogenerated field, which impedes the transport of slower migrating defects like V_{MA}. Excess of Br^- related defects under strong illumination retards

the diffusion of MA^+ towards the interface, so the *D* values decrease. The calculated *D* values from the Warburg element decrease by an order of magnitude as the composition is changed from $MAPbI_3$ (10^{-7} cm^2 s^{-1}) to $MAPbBr_3$ (10^{-8} cm^2 s^{-1}) implying that the diffusing species may be MA^+. Our conclusion is based on the activation energy (E_A) barriers calculated for MA^+, I^- and Br^- in $MAPbI_3$ and $MAPbBr_3$.[11,29] The activation energy barrier for MA^+ migration increases from 0.46 eV in $MAPbI_3$ to 0.56 eV in $MAPbBr_3$ and decreases for halides, 0.16 eV (I^-) in $MAPbI_3$ to 0.09 eV (Br^-) in $MAPbBr_3$. This trend in E_A for ion migration in $MAPbI_3$ and $MAPbBr_3$ is also observed by Grätzel and co-workers.[11] Thus, if we were observing halide diffusion, we would expect *D* values to be higher in $MAPbBr_3$ than $MAPbI_3$. We also calculated the *D* values for $MAPbI_3$ from the method reported by Bisquert and co-workers for probing ion diffusion and found that our *D* values match perfectly with the ones calculated from their method (Table S5).[33] Furthermore, our *D* values are in close agreement with the experimental diffusion coefficients reported in the literature for MA^+.[23,27]

Similarly, IS data for each mixed halide $MAPb(I_{1-x}Br_x)_3$ composition (Figure S4b-e) was fitted with our established equivalent circuit model.[23] An example of the fitted plot for $MAPb(I_{0.8}Br_{0.2})_3$ and the values of circuit parameters for each composition are included as shown in Figure S5b and Table S6, respectively. The *D* values for each mixed halide $MAPb(I_{1-x}Br_x)_3$ composition are plotted as a function of light intensity in **Figure 6**. The *D* values in x= 0.2 match $MAPbBr_3$ under low intensities (10^{-8} cm^2 s^{-1}) but increase a little at higher intensities (10^{-7} cm^2 s^{-1}). Unlike x= 0.2, the mid-range compositions x= 0.4 and 0.6 do not exhibit a clear trend with varying light intensities. Notably, compositions with large Br^- concentration have large *D* values. This observation indicates that increasing the Br^- concentration, in mixed halide compositions, lowers the migration barrier. Low migration barrier in compositions x> 0.2 result from the structural transition from tetragonal

to cubic. As a result of mismatch in the size of halide, the compositions x> 0.2 phase segregate under illumination.[27] The x= 0.4 and 0.6 compositions are expected to phase segregate into two separate regions, an iodide-rich and a bromide-rich region.[34] The phase segregation occurred when the sample was exposed to low light intensity, after which *D* values became constant. We are unable to distinguish the MA^+ diffusion in the iodide-rich and bromide-rich phases at this time because of similar MA^+ diffusion rates; we only observe a single Warburg feature. In conclusion, the trend in *D* values show that phase segregation occurs in x= 0.4 and 0.6 compositions under the employed illumination intensity range whereas in x= 0.2 it does not.[34]

As aforementioned, we expect that the activation energy barrier for Br^- ion transport (0.09 eV) in $MAPbBr_3$ will be lower than that of the I^- (0.16 eV) in $MAPbI_3$.[11,29] Despite the addition of a faster mobile ion (Br^-), analysis of the low-frequency component in the IS resulted in a slower diffusion coefficient for $MAPbBr_3$ devices. Thus, we inferred that the low-frequency component in IS was associated with MA^+/V_{MA} migration. On the other hand, we believe that the high-frequency semicircle in the IS contains information about both the electronic and halide ion/defect relaxation. Therefore, we conclude that stable HOIP devices can be only achieved by impeding the transport of both the organic cation and the halide anion.

Several studies report strategies to mitigate the transport of either the organic cation or the halide through interface engineering,[35,36] minimizing defects,[37,38] incorporating additives[39–41] and mixing various compositions.[42,43] We suggest that ion migration could be attenuated by introducing larger-sized and polar cations that are more sterically bound in the lattice and can interact with the inorganic framework via hydrogen bonding. Recently, Petra and co-workers showed that by introducing larger cations the activation energy barrier for halide diffusion is increased.[31] If this is

true, incorporation of a bulky and polar organic cation will increase the migration barrier for both the A-site cation and halide, resulting in a stable composition under illumination. This opens up an avenue for exploring potential A-site organic cations that could fit in a HOIP lattice and exhibit higher light stability without compromising the device performance. Furthermore, it would be interesting to study the effect of replacing MA^+ with different dipole containing A-site organic cations on the electronic response of the HOIP.[44,45]

CONCLUSIONS

Ion transport has been implicated as the source of instability of PSCs under illumination. Therefore, it is imperative to develop an unequivocal understanding of ion transport so that this problem could be solved. Here, we have investigated the effect of halide substitution in $MAPb(I_{1-x}Br_x)_3$-based devices *in-operando*. We also studied the impact of light intensity and electrical bias on ion transport in these compositions. We found that the concentration of Br^- in the composition significantly alters the resistive and capacitive response under varying light intensity and electrical bias. For example, the recombination resistance (R_{rec}) showed a linear inverse relationship with light intensity in $MAPbI_3$ and $MAPbBr_3$ whereas, the mixed compositions deviated from the linearity upon increasing Br^- concentration. This effect was more prominent under bias where we observed a non-linear decrease in R_{rec} which, interestingly, was more significant in low Br^- compositions *i.e.* $MAPb(I_{0.8}Br_{0.2})_3$ and $MAPb(I_{0.6}Br_{0.4})_3$. This indicates that increasing the Br^- concentration in $MAPb(I_{1-x}Br_x)_3$ favors charge screening. Moreover, contrary to the previous notion about low frequency capacitance, we show that the low frequency capacitance does not increase proportionally with light intensity. Furthermore, we calculated the diffusion coefficient (D) for each $MAPb(I_{1-x}Br_x)_3$ composition under different light intensity and found that the D values decreased on changing the composition from $MAPbI_3$ (10^{-7} cm^2 s^{-1}) to $MAPbBr_3$ (10^{-8} cm^2 s^{-1}). On

the other hand, *D* values increased upon increasing the Br^- concentration in mixed compositions. We believe that the slow ionic response is coupled with the fast-electronic processes, where the increase in Br^- concentration modulates charge transport.

ASSOCIATED CONTENT

X-ray diffraction of $MAPbI_3$, Capacitance as a function of applied bias for $MAPb(I_{0.8}Br_{0.2})_3$ under different light intensities, R_{rec} as a function of bias for mixed halide compositions of $MAPb(I_{1-x}Br_x)_3$, Nyquist plots of $MAPb(I_{1-x}Br_x)_3$ compositions as a function of light intensity, Nyquist plots and equivalent circuit fits for $MAPbI_3$, $MAPb(I_{0.8}Br_{0.2})_3$ and $MAPbI_3$ devices, IS model fit parameters and % error for $MAPbI_3$, IS model fit parameters and % error for $MAPbBr_3$, Comparison of time constants and *D* values calculated from our model and literature, Structure of PVBT-SO_3 and C_{60}-N.

AUTHOR INFORMATION

Corresponding Author

* (D. Venkataraman) E-mail: dv@chem.umass.edu

ORCID

Hamza Javaid: 0000-0002-8845-0676

Monojit Bag: 0000-0002-4210-5455

D. Venkataraman: 0000-0003-2906-0579

Present Addresses

§ Beijing Advanced Innovation Center for Soft Matter Science and Engineering, State Key Laboratory of Chemical Resource Engineering, Beijing University of Chemical Technology Beijing 100029, China

Author Contributions

The manuscript was written through contributions of all authors. All authors have given approval to the final version of the manuscript.

Notes

The authors declare no competing financial interests.

ACKNOWLEDGMENT

Preliminary studies for this work were supported by the Polymer-Based Materials for Harvesting Solar Energy (PHaSE), an Energy Frontier Research Center that was funded by the U.S. Department of Energy, Office of Science, Basic Energy Sciences under Award No. DE-SC0001087. We also gratefully acknowledge the financial support of Army Natick Soldier R D and E Center through contract no. W911QY1820002. We thank the Laboratory for Electronic Materials and Devices of the Institute for Applied Life Sciences at the University of Massachusetts, Amherst. We also thank Professor Todd Emrick for providing PVBT-SO_3 and C_{60}-N interlayers.

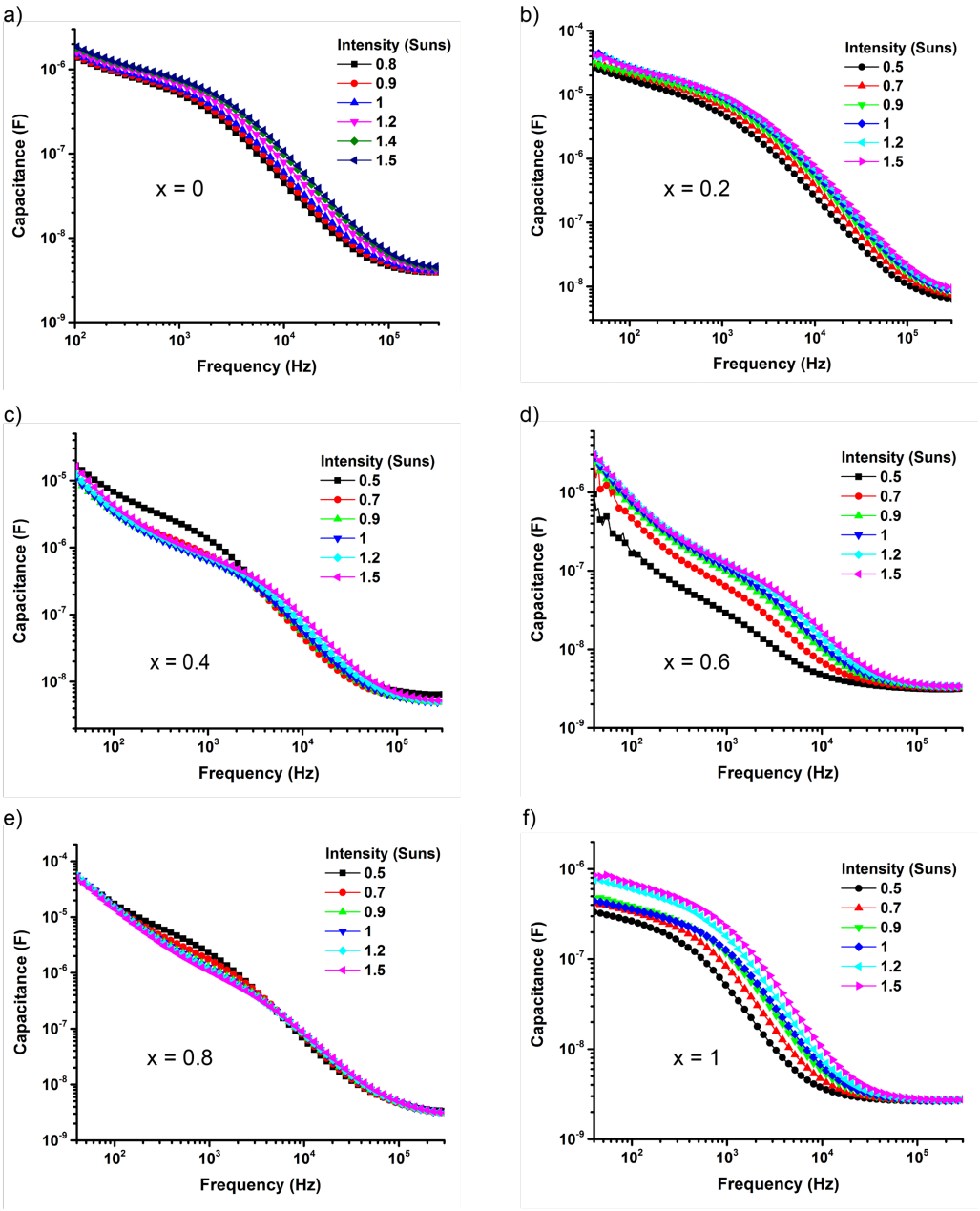

Figure 1. The log-log plot of capacitance and frequency for different compositions of $MAPb(I_{1-x}Br_x)_3$ under various light intensities.

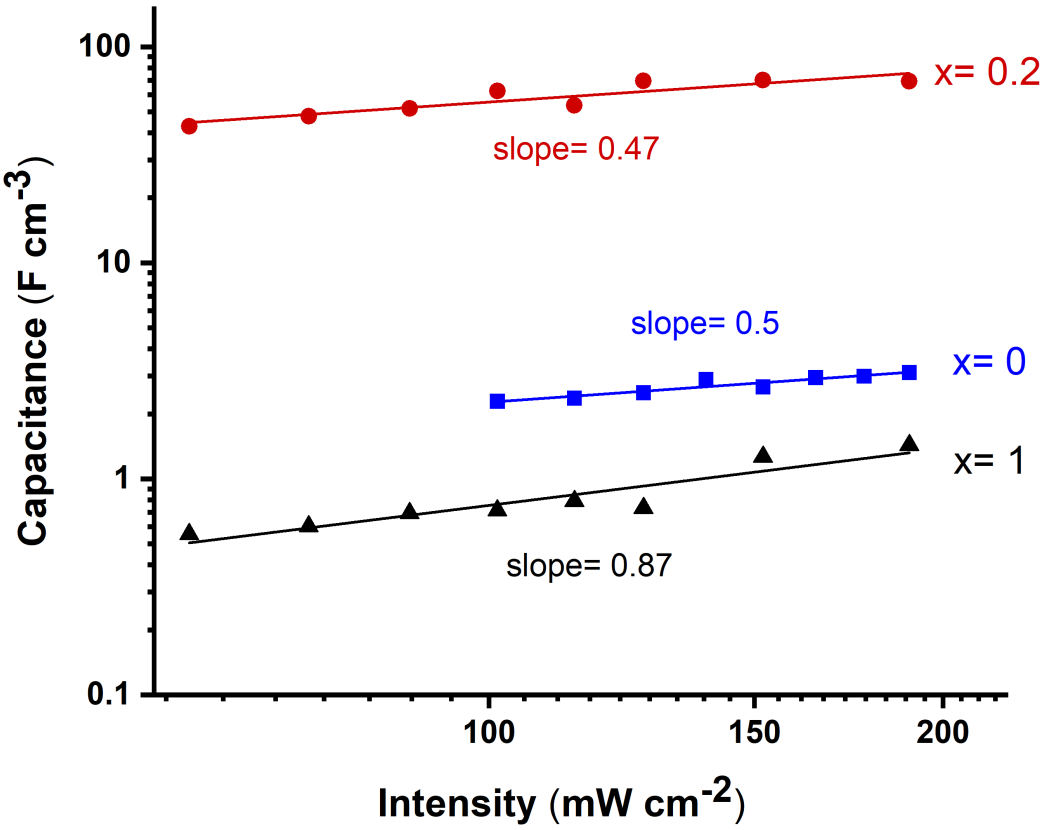

Figure 2. Accumulation capacitance of different $MAPb(I_{1-x}Br_x)_3$ compositions extracted from the low-frequency (< 100 Hz). Capacitance per unit length as a function of the light intensity show the non-proportional dependence with light intensity.

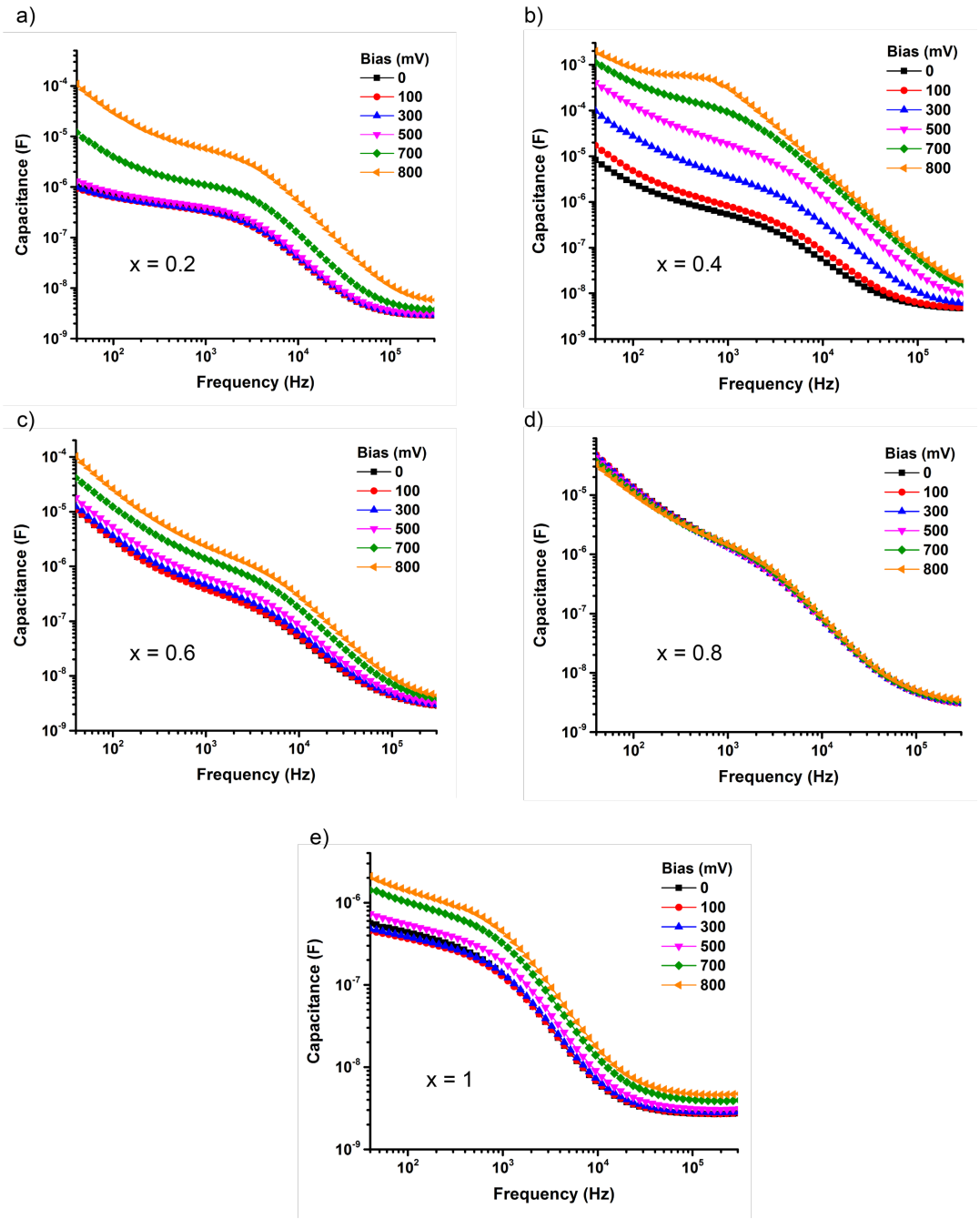

Figure 3. Capacitance spectra measured in short-circuit conditions for different compositions of $MAPb(I_{1-x}Br_x)_3$ under various applied biases.

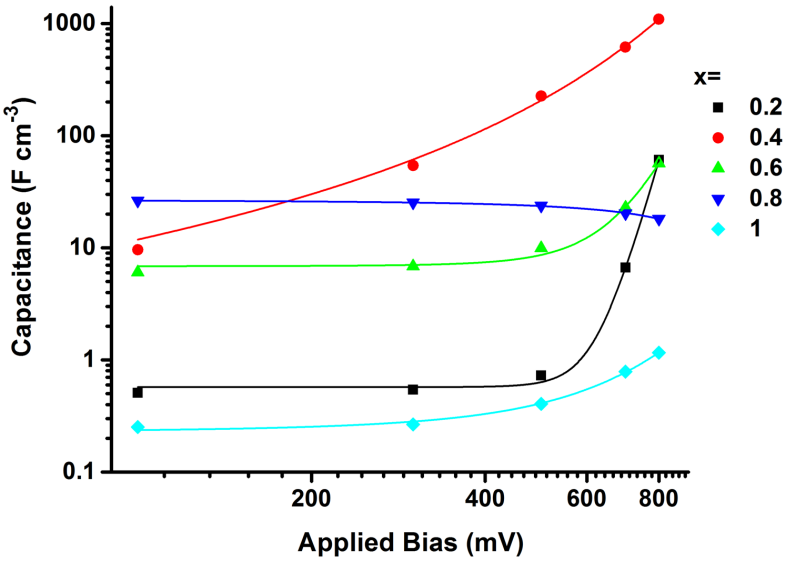

Figure 4. The plot of accumulated capacitance as a function of applied bias in Br^- containing $MAPb(I_{1-x}Br_x)_3$ compositions.

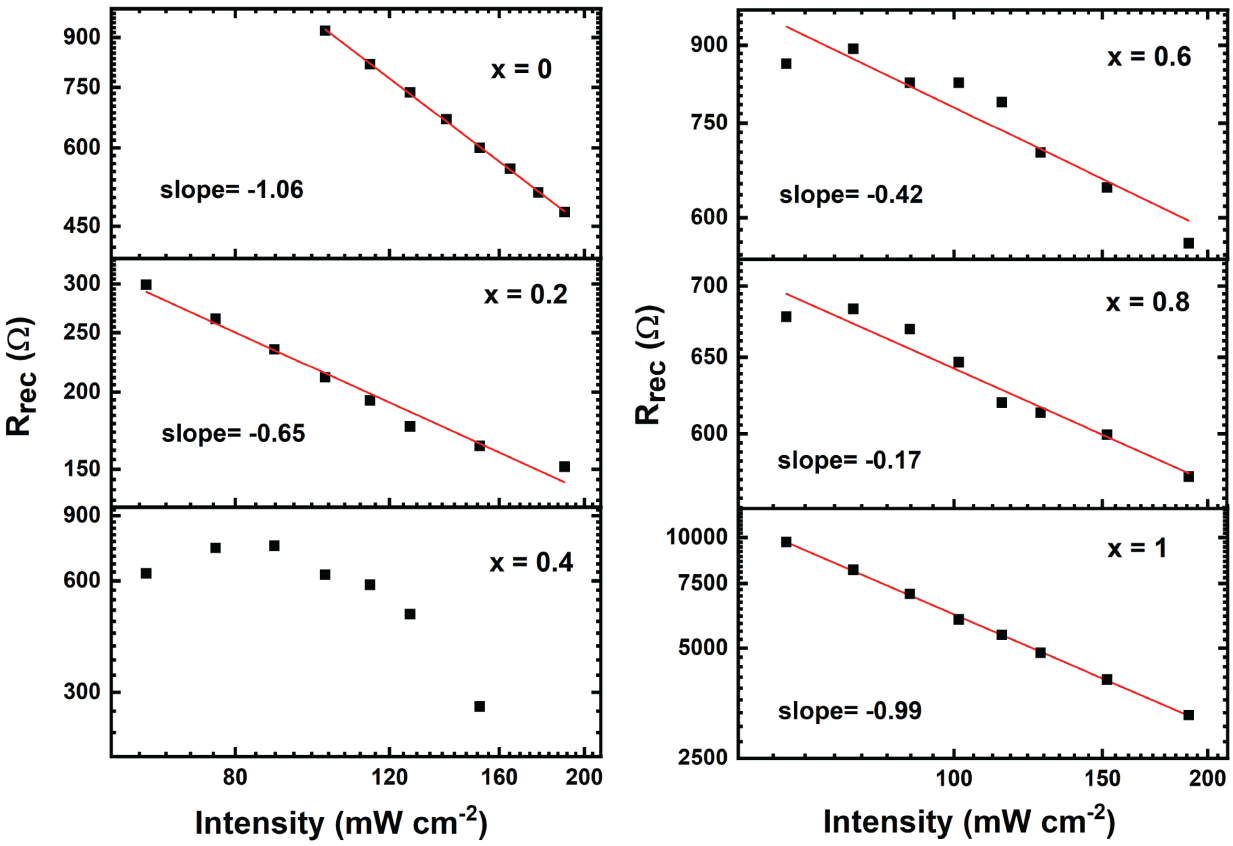

Figure 5. The change in recombination resistance (R_{rec}) as a function of light intensity for $MAPb(I_{1-x}Br_x)_3$ compositions.

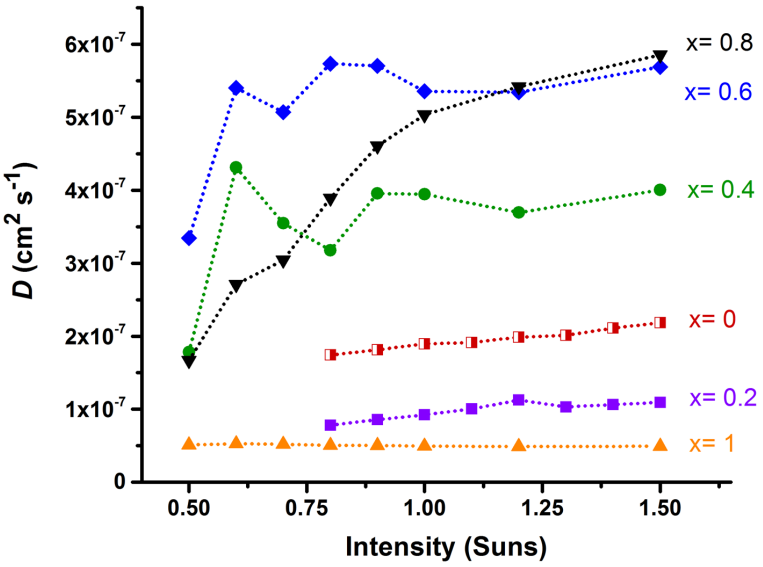

Figure 6. Diffusion coefficient (*D*) for different compositions of $MAPb(I_{1-x}Br_x)_3$ were plotted against light intensity.

REFERENCES

(1) Eames, C.; Frost, J. M.; Barnes, P. R. F.; O'Regan, B. C.; Walsh, A.; Islam, M. S. Ionic Transport in Hybrid Lead Iodide Perovskite Solar Cells. *Nat. Commun.* **2015**, *6*, 7497.

(2) Yang, T.-Y.; Gregori, G.; Pellet, N.; Grätzel, M.; Maier, J. The Significance of Ion Conduction in a Hybrid Organic–Inorganic Lead-Iodide-Based Perovskite Photosensitizer. *Angew. Chemie Int. Ed.* **2015**, *54* (27), 7905–7910.

(3) Calado, P.; Telford, A. M.; Bryant, D.; Li, X.; Nelson, J.; O'Regan, B. C.; Barnes, P. R. F. Evidence for Ion Migration in Hybrid Perovskite Solar Cells with Minimal Hysteresis. *Nat. Commun.* **2016**, *7*, 10.

(4) van Reenen, S.; Kemerink, M.; Snaith, H. J. Modeling Anomalous Hysteresis in Perovskite Solar Cells. *J. Phys. Chem. Lett.* **2015**, *6* (19), 3808–3814.

(5) Yuan, Y.; Huang, J. Ion Migration in Organometal Trihalide Perovskite and Its Impact on Photovoltaic Efficiency and Stability. *Acc. Chem. Res.* **2016**, *49* (2), 286–293.

(6) Huang, J.; Yuan, Y.; Shao, Y.; Yan, Y. Understanding the Physical Properties of Hybrid Perovskites for Photovoltaic Applications. *Nat. Rev. Mater.* **2017**, *2*, 17042.

(7) Deng, Y.; Xiao, Z.; Huang, J. Light-Induced Self-Poling Effect on Organometal Trihalide Perovskite Solar Cells for Increased Device Efficiency and Stability. *Adv. Energy Mater.* **2015**, *5*, 6.

(8) Senocrate, A.; Moudrakovski, I.; Kim, G. Y.; Yang, T.-Y.; Gregori, G.; Grätzel, M.; Maier, J. The Nature of Ion Conduction in Methylammonium Lead Iodide: A Multimethod Approach. *Angew. Chemie Int. Ed.* **2017**, *56* (27), 7755–7759.

(9) Ferdani, D. W.; Pering, S. R.; Ghosh, D.; Kubiak, P.; Walker, A. B.; Lewis, S. E.; Johnson, A. L.; Baker, P. J.; Islam, M. S.; Cameron, P. J. Partial Cation Substitution Reduces Iodide Ion Transport in Lead Iodide Perovskite Solar Cells. *Energy Environ. Sci.* **2019**, *12* (7), 2264–2272.

(10) Brennan, M. C.; Draguta, S.; Kamat, P. V.; Kuno, M. Light-Induced Anion Phase Segregation in Mixed Halide Perovskites. *ACS Energy Lett.* **2018**, *3* (1), 204–213.

(11) Meloni, S.; Moehl, T.; Tress, W.; Franckevičius, M.; Saliba, M.; Lee, Y. H.; Gao, P.; Nazeeruddin, M. K.; Zakeeruddin, S. M.; Rothlisberger, U.; Graetzel, M. Ionic Polarization-Induced Current-Voltage Hysteresis in $CH_3NH_3PbX_3$ Perovskite Solar Cells. *Nat. Commun.* **2016**, *7*, 10334.

(12) Kumar, V.; Schmidt, W. L.; Schileo, G.; Masters, R. C.; Wong-Stringer, M.; Sinclair, D.

C.; Reaney, I. M.; Lidzey, D.; Rodenburg, C. Nanoscale Mapping of Bromide Segregation on the Cross Sections of Complex Hybrid Perovskite Photovoltaic Films Using Secondary Electron Hyperspectral Imaging in a Scanning Electron Microscope. *ACS Omega* **2017**, *2* (5), 2126–2133.

(13) Luo, Y.; Khoram, P.; Brittman, S.; Zhu, Z.; Lai, B.; Ong, S. P.; Garnett, E. C.; Fenning, D. P. Direct Observation of Halide Migration and Its Effect on the Photoluminescence of Methylammonium Lead Bromide Perovskite Single Crystals. *Adv. Mater.* **2017**, *29* (43), 1703451.

(14) Braly, I. L.; Stoddard, R. J.; Rajagopal, A.; Uhl, A. R.; Katahara, J. K.; Jen, A. K.-Y.; Hillhouse, H. W. Current-Induced Phase Segregation in Mixed Halide Hybrid Perovskites and Its Impact on Two-Terminal Tandem Solar Cell Design. *ACS Energy Lett.* **2017**, *2* (8), 1841–1847.

(15) Duong, T.; Mulmudi, H. K.; Wu, Y.; Fu, X.; Shen, H.; Peng, J.; Wu, N.; Nguyen, H. T.; Macdonald, D.; Lockrey, M.; White, T. P.; Weber, K.; Catchpole, K. Light and Electrically Induced Phase Segregation and Its Impact on the Stability of Quadruple Cation High Bandgap Perovskite Solar Cells. *ACS Appl. Mater. Interfaces* **2017**, *9* (32), 26859–26866.

(16) Zarazua, I.; Bisquert, J.; Garcia-Belmonte, G. Light-Induced Space-Charge Accumulation Zone as Photovoltaic Mechanism in Perovskite Solar Cells. *J. Phys. Chem. Lett.* **2016**, *7* (3), 525–528.

(17) Juarez-Perez, E. J.; Sanchez, R. S.; Badia, L.; Garcia-Belmonte, G.; Kang, Y. S.; Mora-Sero, I.; Bisquert, J. Photoinduced Giant Dielectric Constant in Lead Halide Perovskite Solar Cells. *J. Phys. Chem. Lett.* **2014**, *5* (13), 2390–2394.

(18) Weller, M. T.; Weber, O. J.; Henry, P. F.; Di Pumpo, A. M.; Hansen, T. C. Complete Structure and Cation Orientation in the Perovskite Photovoltaic Methylammonium Lead Iodide between 100 and 352 K. *Chem. Commun.* **2015**, *51*, 4180–4183.

(19) Wang, K. H.; Li, L. C.; Shellaiah, M.; Wen Sun, K. Structural and Photophysical Properties of Methylammonium Lead Tribromide (MAPbBr3) Single Crystals. *Sci. Rep.* **2017**, *7* (1), 14.

(20) Kumar, R.; Kumar, J.; Srivastava, P.; Moghe, D.; Kabra, D.; Bag, M. Unveiling the Morphology Effect on the Negative Capacitance and Large Ideality Factor in Perovskite Light-Emitting Diodes. *ACS Appl. Mater. Interfaces* **2020**, *12* (30), 34265–34273.

(21) Pockett, A.; Eperon, G. E.; Peltola, T.; Snaith, H. J.; Walker, A.; Peter, L. M.; Cameron, P. J. Characterization of Planar Lead Halide Perovskite Solar Cells by Impedance Spectroscopy, Open-Circuit Photovoltage Decay, and Intensity-Modulated Photovoltage/Photocurrent Spectroscopy. *J. Phys. Chem. C* **2015**, *119* (7), 3456–3465.

(22) Guerrero, A.; Garcia-Belmonte, G.; Mora-Sero, I.; Bisquert, J.; Kang, Y. S.; Jacobsson, T. J.; Correa-Baena, J.-P.; Hagfeldt, A. Properties of Contact and Bulk Impedances in Hybrid Lead Halide Perovskite Solar Cells Including Inductive Loop Elements. *J. Phys. Chem. C* **2016**, *120* (15), 8023–8032.

(23) Bag, M.; Renna, L. A.; Adhikari, R.; Karak, S.; Liu, F.; Lahti, P. M.; Russell, T. P.; Tuominen, M. T.; Venkataraman, D. Kinetics of Ion Transport in Perovskite Active Layers and Its Implications for Active Layer Stability. *J. Am. Chem. Soc.* **2015**, *137*, 13130–13137.

(24) Pockett, A.; Eperon, G. E.; Sakai, N.; Snaith, H. J.; Peter, L. M.; Cameron, P. J.

Microseconds, Milliseconds and Seconds: Deconvoluting the Dynamic Behaviour of Planar Perovskite Solar Cells. *Phys. Chem. Chem. Phys.* **2017**, *19* (8), 5959–5970.

(25) Moia, D.; Gelmetti, I.; Calado, P.; Fisher, W.; Stringer, M.; Game, O.; Hu, Y.; Docampo, P.; Lidzey, D.; Palomares, E.; Nelson, J.; Barnes, P. R. F. Ionic-to-Electronic Current Amplification in Hybrid Perovskite Solar Cells: Ionically Gated Transistor-Interface Circuit Model Explains Hysteresis and Impedance of Mixed Conducting Devices. *Energy Environ. Sci.* **2019**, *12* (4), 1296–1308.

(26) Smith, E. C.; Ellis, C. L. C.; Javaid, H.; Renna, L. A.; Liu, Y.; Russell, T. P.; Bag, M.; Venkataraman, D. Interplay Between Ion Transport, Applied Bias and Degradation under Illumination in Hybrid Perovskite p-i-n Devices. *J. Phys. Chem. C* **2018**, *122*, 13986–13994.

(27) Liu, Y.; Renna, L. A.; Thompson, H. B.; Page, Z. A.; Emrick, T.; Barnes, M. D.; Bag, M.; Venkataraman, D.; Russell, T. P. Role of Ionic Functional Groups on Ion Transport at Perovskite Interfaces. *Adv. Energy Mater.* **2017**, *7*, 13.

(28) Lvovich, V. F. *Impedance Spectroscopy: Applications to Electrochemical and Dielectric Phenomena*; Wiley, 2012.

(29) Azpiroz, J. M.; Mosconi, E.; Bisquert, J.; De Angelis, F. Defect Migration in Methylammonium Lead Iodide and Its Role in Perovskite Solar Cell Operation. *Energy Environ. Sci.* **2015**, *8* (7), 2118–2127.

(30) Yuan, Y.; Chae, J.; Shao, Y.; Wang, Q.; Xiao, Z.; Centrone, A.; Huang, J. Photovoltaic Switching Mechanism in Lateral Structure Hybrid Perovskite Solar Cells. *Adv. Energy Mater.* **2015**, *5*, 7.

(31) Lewis, S. E.; Johnson, A. L.; Baker, P. J.; Islam, M. S.; Petra, J.; Page, A. M. Partial Cation Substitution Reduces Iodide Ion Transport in Lead Iodide Perovskite Solar Cells. **2019**, *7* (C), 1–33.

(32) Chen, X.; Shirai, Y.; Yanagida, M.; Miyano, K. Effect of Light and Voltage on Electrochemical Impedance Spectroscopy of Perovskite Solar Cells: An Empirical Approach Based on Modified Randles Circuit. *J. Phys. Chem. C* **2019**, *123* (7), 3968–3978.

(33) Peng, W.; Aranda, C.; Bakr, O. M.; Garcia-Belmonte, G.; Bisquert, J.; Guerrero, A. Quantification of Ionic Diffusion in Lead Halide Perovskite Single Crystals. *ACS Energy Lett.* **2018**, *3* (7), 1477–1481.

(34) Hoke, E. T.; Slotcavage, D. J.; Dohner, E. R.; Bowring, A. R.; Karunadasa, H. I.; McGehee, M. D. Reversible Photo-Induced Trap Formation in Mixed-Halide Hybrid Perovskites for Photovoltaics. *Chem. Sci.* **2015**, *6* (1), 613–617.

(35) Bai, Y.; Meng, X.; Yang, S. Interface Engineering for Highly Efficient and Stable Planar P-i-n Perovskite Solar Cells. *Adv. Energy Mater.* **2018**, *8* (5), 1701883.

(36) Yang, G.; Wang, C.; Lei, H.; Zheng, X.; Qin, P.; Xiong, L.; Zhao, X.; Yan, Y.; Fang, G. Interface Engineering in Planar Perovskite Solar Cells: Energy Level Alignment, Perovskite Morphology Control and High Performance Achievement. *J. Mater. Chem. A* **2017**, *5* (4), 1658–1666.

(37) Wang, F.; Bai, S.; Tress, W.; Hagfeldt, A.; Gao, F. Defects Engineering for High-Performance Perovskite Solar Cells. *npj Flex. Electron.* **2018**, *2* (1), 22.

(38) Son, D.-Y.; Kim, S.-G.; Seo, J.-Y.; Lee, S.-H.; Shin, H.; Lee, D.; Park, N.-G. Universal

Approach toward Hysteresis-Free Perovskite Solar Cell via Defect Engineering. *J. Am. Chem. Soc.* **2018**, *140* (4), 1358–1364.

(39) Bai, S.; Da, P.; Li, C.; Wang, Z.; Yuan, Z.; Fu, F.; Kawecki, M.; Liu, X.; Sakai, N.; Wang, J. T.-W.; Huettner, S.; Buecheler, S.; Fahlman, M.; Gao, F.; Snaith, H. J. Planar Perovskite Solar Cells with Long-Term Stability Using Ionic Liquid Additives. *Nature* **2019**, *571* (7764), 245–250.

(40) Hu, Y.; Hutter, E. M.; Rieder, P.; Grill, I.; Hanisch, J.; Aygüler, M. F.; Hufnagel, A. G.; Handloser, M.; Bein, T.; Hartschuh, A.; Tvingstedt, K.; Dyakonov, V.; Baumann, A.; Savenije, T. J.; Petrus, M. L.; Docampo, P. Understanding the Role of Cesium and Rubidium Additives in Perovskite Solar Cells: Trap States, Charge Transport, and Recombination. *Adv. Energy Mater.* **2018**, *8* (16), 11.

(41) Zhang, F.; Zhu, K. Additive Engineering for Efficient and Stable Perovskite Solar Cells. *Adv. Energy Mater.* **2020**, *10* (13), 1902579.

(42) Kubicki, D. J.; Prochowicz, D.; Hofstetter, A.; Saski, M.; Yadav, P.; Bi, D.; Pellet, N.; Lewiński, J.; Zakeeruddin, S. M.; Grätzel, M.; Emsley, L. Formation of Stable Mixed Guanidinium–Methylammonium Phases with Exceptionally Long Carrier Lifetimes for High-Efficiency Lead Iodide-Based Perovskite Photovoltaics. *J. Am. Chem. Soc.* **2018**, *140* (9), 3345–3351.

(43) Salado, M.; Jodlowski, A. D.; Roldan-Carmona, C.; de Miguel, G.; Kazim, S.; Nazeeruddin, M. K.; Ahmad, S. Surface Passivation of Perovskite Layers Using Heterocyclic Halides: Improved Photovoltaic Properties and Intrinsic Stability. *Nano Energy* **2018**, *50*, 220–228.

(44) Bakulin, A. A.; Selig, O.; Bakker, H. J.; Rezus, Y. L. A.; Müller, C.; Glaser, T.; Lovrincic, R.; Sun, Z.; Chen, Z.; Walsh, A.; Frost, J. M.; Jansen, T. L. C. Real-Time Observation of Organic Cation Reorientation in Methylammonium Lead Iodide Perovskites. *J. Phys. Chem. Lett.* **2015**, *6* (18), 3663–3669.

(45) Wilson, J. N.; Frost, J. M.; Wallace, S. K.; Walsh, A. Dielectric and Ferroic Properties of Metal Halide Perovskites. *APL Mater.* **2019**, *7* (1), 10901.